Desalination and Purification of Water using a Solar Powered Hydrogel Multistage

Kevin Murphy
Mr. Kemp, Dr. Chen & Dr. Bleckner
Princeton International School of Mathematics and Science, Spring 2022

Abstract

One third of humanity is without access to clean drinking water. Additionally, over 90% of clean drinking water is contaminated with microplastics. 71% of the earth's surface is water but we are without a cheap, efficient and versatile means of making water safe to drink. This study aims to design, build and test a highly efficient, solar powered and portable water purification method that will cleans water of most contaminants, including microplastics, salt and pathogens, and can be used across the globe. In this study a water vaporization enthalpy decreasing hydrogel was synthesized and both dehydration and freeze drying techniques were tested and compared in stimulating the expansion of hydrophilic pores within the hydrogel. These pores are capable of manipulating the hydrogen bonding within the water molecules resulting in a lower evaporation enthalpy. Prior studies that freeze dried at -196°C have indicated a reduction of upto 58.8% however this study freeze dried the hydrogels at -80°C and will be tested using a differential scanning calorimeter. These hydrogels were stacked in a multistage consisting of silicone, semipermeable membranes and aluminum in order to increase the heat efficiency of the design by up to 450%. In order to power the system a solar tracking mylar coated nested paraboloidal solar collector capable of capturing 223.8W has been designed to float on the water's surface and fuel the multistage via heat pipe. The unity of these industry leading concepts enables the proposed system to reliably evaporate and purify water while reducing the energy cost of evaporative desalination from 2260 J g^{-1} to 232.75 J g^{-1} and running on renewable energy. This study's prototype is capable of sustaining a theoretical purification rate of 4.02 L hr^{-1} per hour and an evaporation rate of 402L hr^{-1} m^{-2} enabling it to purify water indefinitely.

Introduction

The United Nations has a goal to supply clean water and sanitation for all [1]. This goal originates from the fact that one in three people do not have access to safe drinking water [1]. Clean water is an essential resource for our survival, yet of the 3% of water on Earth that is fresh only 0.5% is drinkable [2]. As well as this, our already meager water resources are being threatened by climate change as weather patterns change and sea levels rise [3]. For example, San Diego's water is supplied by the Colorado River but, due to a change in weather patterns, the water level is dropping resulting in a need to look elsewhere for clean water [4]. This lack of clean water will likely become more widespread and even amplified as our climate becomes less stable due to catastrophes, such as the deforestation of the Amazon[5].

To tackle water shortages, desalination plants are being built. However, the process is inhibited by high operating costs. For example, plants spend 1,000 to 2,000 US dollars per acre-foot (of water), $10's to $100's of millions per year in maintenance, and billions in construction costs [4]. The cost of these plants make them simply out of the question for many impoverished developing countries. The most widely used methods of desalination are reverse osmosis and thermal evaporation [4]. Thermal desalination is typically not commercially viable due to its intensive energy requirement resulting in reverse osmosis plants becoming the favored design. However, reverse osmosis plants have many consequences such as toxic waste pollution and killing of local wildlife [4]. Even our supposedly safe drinking water is at risk as microplastics have been found in over 90% of all drinkable water[6]. Microplastics have the potential to cause health problems such as cancer, weakened immune systems and reproductive problems [7]. The water industry is crucial to humanity's survival, yet it has so much room for improvement.

Theory

This study aims to synthesize hydrogels that decrease the enthalpy of both saltwater and freshwater vaporization by about half [8]. The hydrogel reduces water vaporization enthalpy because of the hydrophilic bonds between both Chitosan & Polyvinyl Alcohol with water [8]. These hydrophilic bonds weaken the hydrogen bonding within the water, labeled in Figure 1 as “Intermediate water”, reducing their enthalpy of vaporization from 2260 J g^{-1} to 931J g^{-1} as shown in Figure 3 [8]. Pores that work as crosslinks enable this type of bonding shown in Figure 1. These pores are generated by repeated freeze-drying of the hydrogel. Freeze-drying is effectively the freezing of water molecules within the hydrogel and the sublimation of these water molecules under vacuum so that porous gaps are left within the hydrogel. The hydrogel utilized a Chitosan and Polyvinyl alcohol mixture of concentration 1.0:0.175 PVA/Chitosan, named h-LAH 4 shown in Figure 3. h-LAH 4 was chosen over h-LAH5 as the saturated water content of h-LAH5 hindered the evaporation enthalpy unpredictably. This was likely due to flooding which overwhelmed the bonding capability of the Chitosan & PVA crosslinks within the hydrogel.

In this study however, the hydrogel was tested by being frozen at a temperature of -80°C and then both dehydrated at 60°C and also being freeze-dried at -80°C as well. This differs from prior research as the hydrogel was frozen in liquid nitrogen at -196°C and freeze-dried [8]. The purpose of testing dehydration was for convenience sake as freeze-dryers are expensive. Additionally, freeze-drying at -80°C has been proven in prior research to increase the pore sizes within Chitosan based hydrogels, as shown in Figure 2. The purpose of changing the pore size was to test if larger pores would decrease the evaporation enthalpy of water within the hydrogel further.

Figure 1: Function of crosslink within Hydrogel

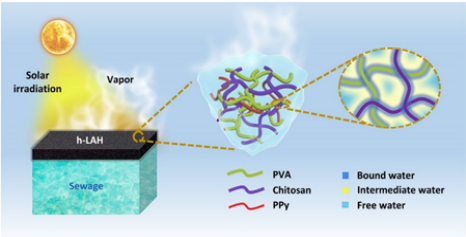

The crosslink effectively induces low bond strength in the Intermediate water via the pull on the bound water. Source 8.

Figure 3: Chitosan Hydrogel freeze-dry -80°C vs -196°C

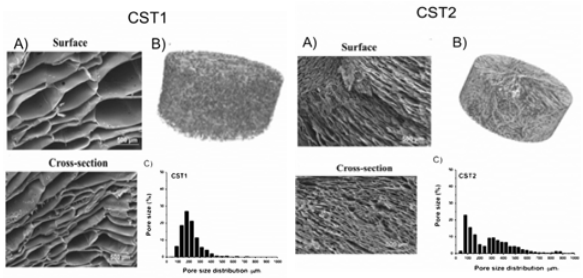

The images above compare the pore distribution and size with differing temperatures of freeze drying, CST1 being -80°C & CST2 being -196°C. Source 9.

Figure 3: Effect of Concentrations of h-LAH

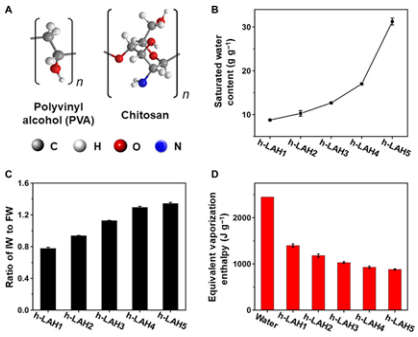

h-LAH 4 with a concentration of 1.0:0.175 PVA: Chitosan was chosen for this study. Source 8.

A multistage was included in the design to increase the efficiency of the system. Generally, in evaporative water purification, the steam generated by water vapor is collected and then condensed. However, the heat retained by the steam is rarely harnessed which wastes potential energy efficency. So, instead of wasting energy, a second stage capable of capturing the heat within that steam and using it to power evaporation would increase the efficiency of the energy put into the system. Adding a third stage would increase the efficiency further still by utilizing the steam of the second stage. This can theoretically go on infinitely but for this project a total of 10 stages were used. Using prior research as reference, use of ten multistages is projected to increase the heat efficiency of the system by up to 450% [10].

This study’s approach to the multistage is different to prior research in that, instead of using a horizontal plane for the travel of water vapor, a vertical plane was used as shown in Figure 4 and Figure 5. A vertical plane was used to minimize heat loss to surrounding walls as heat rises and in prior research a core limitation was the loss of heat

to the surrounding wall. However, where previous research used polyisocyanurate foam as an insulator, this study used silicone due to its high thermal resistance and natural sealing ability. Additionally, the capillary wicks utilized in prior research were replaced with the enthalpy decreasing hydrogels which are described above.

Figure 4: Design and Function of MIT's Multistage

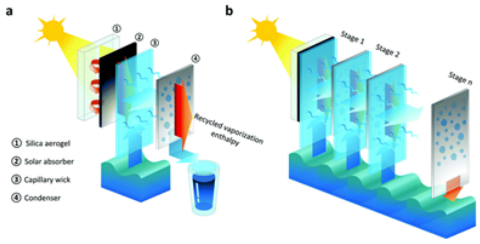

A solar absorber insulated by silica gel heats the first stage of the multistage. The multistage then vaporizes the water drawn by the capillary wick which heats the next stage. Source 10.

Figure 5: Design and Function of this Study's Multistage

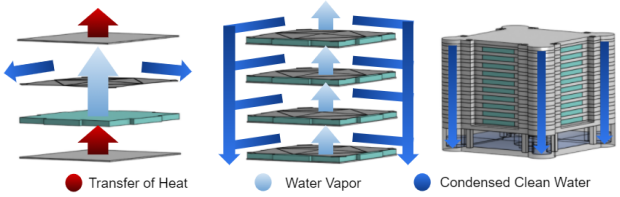

The bottom aluminum plate is heated, evaporating the water within the Hydrogel. Water vapor then passes through the GORE TEX layer and condensates on the next aluminum plate heating it. The condensed water is then caught and funneled by the GORE-TEX into the corners for collection.

To power the multistage a solar tracker was added to the design. The nested paraboloid design was mathematically proven, as shown in Figure 6, to concentrate solar energy from a 0.55 meter diameter outer parabola into a 10 cm diameter. Beneath the diameter is a 150mm diameter lens with a focal length of 70 mm. The lens focuses the light onto a central absorber 2cm in diameter which is connected to the bottom stage of the multistage via thermal piping. An automated slider, as shown in Figure 7, sits below the nested paraboloids to avoid the system overheating. The solar collector is also automated to be capable of solar tracking anywhere in the world. The collector is mounted on a pair of arms that are in turn mounted on a geared turntable allowing 90° of rotation combined with 360° of rotation for differing distances from the equator as shown in Figure 7. An Arduino determines location and necessary movement in relation to the sun through a photoresistor circuit in a constant feedback loop. The same Arduino also controls the motors connected to the arm, turntable, and slider.

Figure 6: Calculation and graphing of light trajectory within reflective Paraboloids

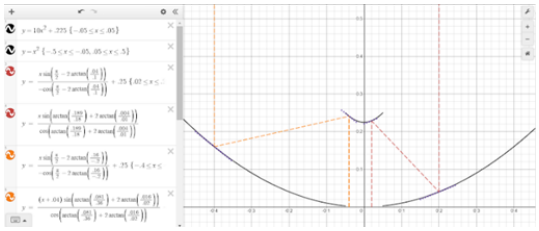

Tangent line, angle of incidence and equation of reflected ray were calculated showing the function of the reflective nested paraboloids. Thanks to Dr. Bleckner for checking calculations.

Figure 7: Solar Tracker range of movement

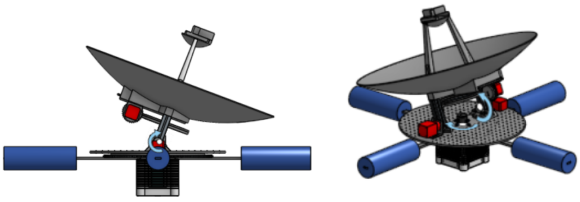

The first image shows 90° of arm movement and the second shows 360° of turntable rotation. These were drawn using Onshape Cad.

Methods & Results

Using the h-LAH4 concentration, 4.25g of PVA, 0.75g mg of Chitosan, 50ml of deionized water and 5 ml of 1.2M Hydrochloric acid were added to a beaker and the solution was then sonicated for approximately 24 hours for thorough dissolution. Once sonicated, 625 µL of glutaraldehyde was added to 50ml of the h-LAH4 solution to strengthen the bonds between the Chitosan/PVA crosslinks. The solution was then poured into a mold and left to gelate into a functional hydrogel. Once the bonds had formed the pre-freeze-dried sample was photographed at 40x zoom under a microscope and hydrated with deionized water before being frozen at a temperature of -80°C. The hydrogel was then reheated at 60°C in a water bath for 30 minutes. The process of freezing at -80°C and heating at 60°C for 30 minutes was repeated for a total of 10 dehydration cycles. Microscopic images of the polymer of 10x strength were taken after the dehydration process. The results of the dehydration process are shown

in Figure 8. While there is distinct progression throughout the process of dehydration (shown in Figure 10) shown in Figure 8*, it does not resemble the consistent porous structure shown in Figures 3 & 9. Additionally, as shown in Figure 11, the dehydrated hydrogels appear disfigured and remain in this shape despite being submerged in and absorbing deionized water.

Figure 8: Image taken after Dehydration of Hydrogel

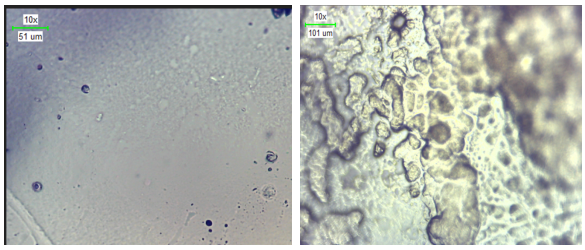

The image on the left is before dehydration and the image ont eh left is after 10 cycles of dehydration. Images show the change in the Hydrogel during the Dehydration process

Figure 9: Porous Hydrogel Freeze Dried 10 times in Liquid Nitrogen in prior study

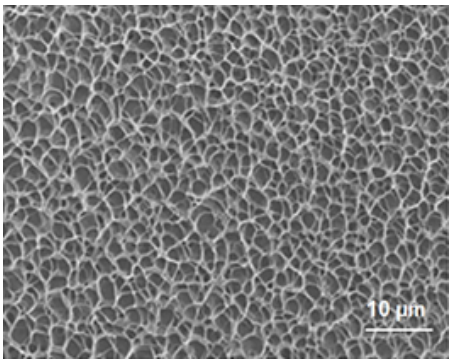

This is an image of h-LAH4 after 10 freeze-dries at -196°C. Source 6.

Figure 10: Dehydration of Hydrogels

Image seen on the left is of hydrogel after being frozen at -80°C and on the right is of hydrogel after the first cycle of dehydration. This study.

Figure 11: Structural perspective of Dehydrated Hydrogels

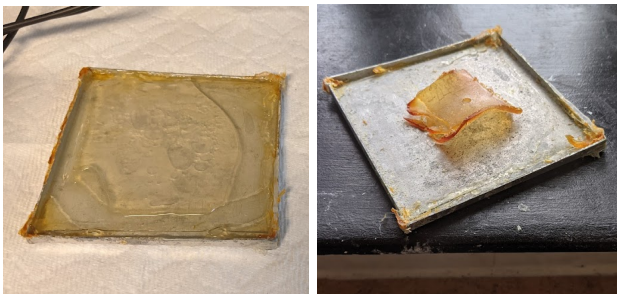

Image seen on the left is of hydrogel before dehydration and on right is of hydrogel after dehydration. This study.

Due to these results a freeze-dryer was constructed so that the differences between dehydration and freeze-drying could be fully tested. The freeze-dryer is shown in Figure 12. The freeze dryer was constructed using a vacuum pump, two vacuum chambers, one being for the sample and the other serving as a water trap, and styrofoam insulation. A hydrogel was synthesized in the same fashion as those that underwent dehydration except where the dehydrated hydrogels underwent 10 cycles in the ventilated incubator, the freeze-dried hydrogel was only freeze-dried once. The results of this process are shown in Figure 13. The freeze-dried hydrogel on the microscopic level resembles the consistent porous structure shown in Figures 3 & 9 and on a structural level the hydrogel retained its original shape and size where the dehydrated sample deformed.

Figure 12: Freeze-Dryer constructed as part of the study

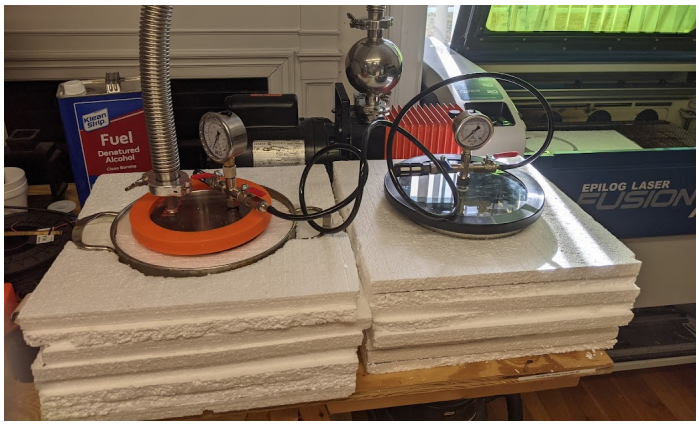

The vacuum pump can be seen in the back, the water trap is on the front left submerged in a cryotank of -80°C and the sample chamber is shown on the front right. This study.

Figure 13: Freeze-Dried Hydrogel

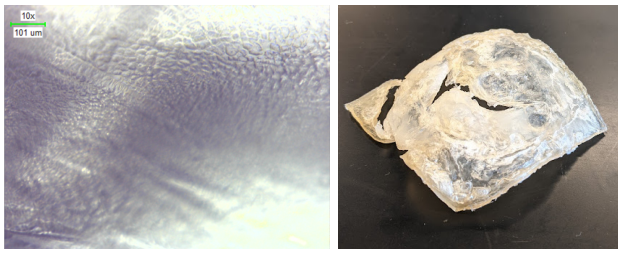

Image seen on the left is a microscopic image and on the right is a structural image of the hydrogel after being frozen at -80°C and freeze-dried. This study

In order to test the evaporation enthalpy of these hydrogels an experiment was set up wherein the hydrated hydrogel's evaporation enthalpy was compared with that of pure water, as seen in Figure 14. This experiment was unfortunately highly inaccurate as there was no way to isolate the hydrogel. In order to compensate for the hydrogels lack of surface area it was submerged in water. However even with this the hydrogel showed impressive results and evaporated 2.25 times as much water as the only water control sample. This allows us to approximate a evaporation enthalpy decrease of ~ 55.5% and by using 2260 J g^{-1} as a reference the approximate evaporation enthalpy would be 1,006 J g^{-1}. Additionally, the hydrogel was recorded to have an evaporation rate of 0.067ml min^{-1} cm^{-2} which is equal to 40.2 L hr^{-1} m^{-2} However this is only an estimate with high potential for inaccuracy. Future experiments aim to achieve a more accurate estimate of the hydrated hydrogels' evaporative enthalpy by using a differential scanning calorimeter.

Figure 14: Experimental setup for comparing evaporation enthalpy

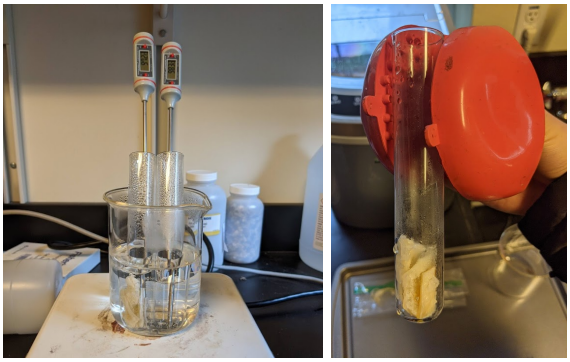

A hot water bath was placed on a hot plate. Within that bath two tubes were placed inside, one with just water (right) and other with water and the hydrogel (left). The second photo is a close up of the hydrogel tube.

The multistage was constructed using a variety of materials. Aluminum plates were used as a conductive intermediate to avoid the hydrogels situated above absorbing the condensed water vapor of the previous stage while still efficiently conducting the energy retained by the water vapor. A GORE-TEX sheet was used as a semipermeable membrane and place between an arched PETG lower clamp and an acrylic upper clamp to facilitate the funneling of the clean condensed water to the corner funnels while also allowing the water vapor to pass through unobstructed. This design avoids the possibility of the hydrogel reabsorbing clean water which would be counterproductive. The surrounding material was made by setting silicone in a 3D printed mold as shown in Figure 16 The semipermeable membrane and aluminum plate were then set into the stage as shown in Figure 17. The silicone not only has low thermal conductivity and high thermal resistance, but it also acts as a natural seal and when under compression ensures that the multistage is watertight as seen in Figure 18.

Figure 15: Single stage design

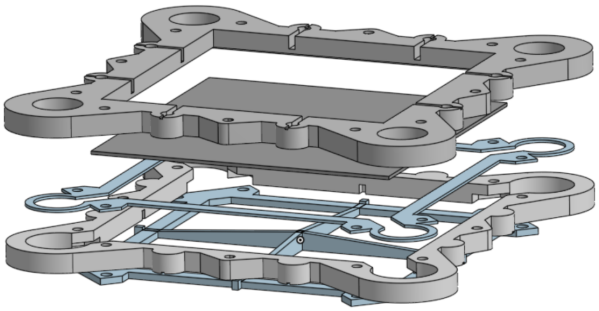

The stage comes together and is capable of stacking with other stages.

Figure 16: Pouring of silicone into molds to create stages

Silicone was poured into 3D printed molds to form the stages used to hold the aluminum plates and semipermeable membranes. They were left to set for 12 hours before being removed.

Figure 17: Single stage parts & assembly

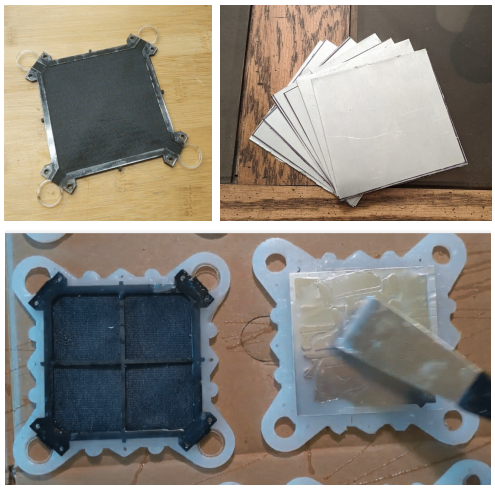

The gore tex layer (top left) and the aluminum sheets (top right) are set into their respective silicone stages. This stage is capable of stacking with other stages.

Figure 18: Constructed Multistage

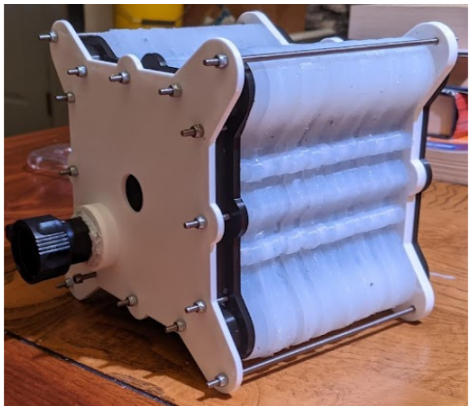

By 3D printing an upper clamp and a lower water storage/ release valve and using them to compress the stages the multistage is constructed and functional.

The solar tracker was constructed by 3D printing multiple pieces of the primary paraboloid and then using a 3D print pen to weld them together. The slider and gear headed stepper motor were connected to the underside of the primary parabola. The secondary paraboloid was also 3D printed and suspended at the focal point of the primary paraboloid using HDPE plastic that was laser cut. Both the primary and secondary paraboloid were coated in Mylar using a heat gun and mylar sheets which offer ~97% reflectivity. The primary paraboloid was screwed into 80-20 10cm aluminum one of which was mounted to a stepper motor and the other was mounted to a pillow block mount. The stepper motor and pillow blocks were bolted to a HDPE turntable top approximately 40cm in diameter. The turntable also supported the Arduino, 3 tic t500s, a thermal absorber and a secondary stepper motor for controlling rotation upon the turntable. The turntable was connected to the underside of the mount and the topside of the geared base with which the turntable top's secondary motor rotated using a gear head. The geared base was also connected to a floating stabilizer that has four arms connected to pool noodles enabling the multistage to be submerged while keeping the solar concentrator above water. A photoresistor circuit was positioned on the secondary paraboloid allowing detection of the sun in relation to the primary paraboloid's focus. Using triangulation, the Arduino can determine and execute movement of the stepper motors to orient the paraboloid at the position of optimal solar collection. The Arduino also controls the slider and uses it to manage the heat of the system which it detects via a thermometer connected to the thermal absorber. The solar collection capability of this design is 223.8W as shown by the calculation:

$$\pi((0.275m)^2 - (0.05m)^2) \cdot \left(\frac{1000W}{m^2}\right) \cdot (97\%) \approx 222.8W$$

The full design is shown in Figure 19.

Figure 19: Study's final design

Image taken in Lawrence Township, New Jersey. This study.

Discussion

The predicted solar thermal efficiency of the multistage, η, can be calculated using the equation

$$\eta = \frac{\dot{m} h_{fg}}{q''_{solar} A} \quad [10]$$

where h_{fg} is the enthalpy of water vaporization, $\dot{m}$ is the vapor production rate under steady state, q''_{solar} is the input solar flux (1000 W m^{-2}), and A is the effective solar

absorbing area. The calculated efficiency for a system where the air gap is ≤ 2.5mm and has 10 stages is ~450% [10]. However, due to a difference in insulation material of, prior study using insulation with thermal conductivity of 0.022 W m^{-1} K^{-1} and current study using insulation of ~0.2 W m^{-1} K^{-1}, and also a difference in orientation, prior study being horizontal and current study being vertical, there may be a slight variance in predicted and actual efficiency.

The hydrogel met expectations in pore size and distribution in that the -80°C freeze dried hydrogel had a consistent pore distribution and greater pore size than the -196°C freeze dried hydrogel as predicted by Source 9. The exact effect of the -80°C freeze-dried hydrogel on the vaporization enthalpy is unknown at this point as a more accurate test needs to be conducted to gain an accurate estimation. However, it does clearly reduce the vaporization enthalpy as shown in the experiment described in Figure14. However, according to the experiment described in Figure 14, the -80°C freeze-dried hydrogel does decrease the evaporation enthalpy and, through further investigation using a differential scanning calorimeter, a more accurate estimate of the hydrogels evaporation enthalpy will be taken.

Due to the PETG lower semipermeable membrane clamp being a limiting factor and having a melting point of 260°C, the ideal max temperature of the first stage of the multistage is 100°C to 150°C. The hydrogel's heat of deformation was also tested up to the temperature of 200°C and it showed no damage.

In order to approximate the production rate of the system both the evaporation enthalpy and the evaporation rate determined in the experimental setup shown in Figure 14 can be used. By using the hydrogels evaporation rate of 40.2 L hr^{-1} m^{-2} and applying it to the prototypes multistage design shown in Figure 5, the expected evaporation rate of the functioning prototype becomes 4.02 L hr^{-1} once all stages are functioning fully.

We can calculate the energy cost of both heating the system initially and maintaining this evaporation rate using the equation:

$$Q=mc\Delta T \qquad [11]$$

where m is the aluminum plate's weight of approximately 26.17g, ΔT is (150°C - 20°C) and c is aluminum's specific heat of 0.900 J g^{-1} $°C^{-1}$, the initial energy requirement, Q, was calculated as 3,062 J.

To calculate the ongoing energy requirement the evaporation rate of the first stage can be multiplied by the experimentally determined evaporation enthalpy of the hydrogel, 1,006 J g^{-1}, giving a requirement of 112.3 Watts a value that the paraboloidal mirror system is more than capable of sustaining with 222.8W. So much so that the paraboloidal mirror can support an additional multistage if they were situated below the solar tracker. This would increase the production rate proportionately with the increased surface area.

Adaptable heat regulation within the system is possible because of the slider mechanism attached to the primary paraboloid which is controlled via the thermometer informed Arduino. The paraboloidal concentrator supplies a maximum of 223.8W to the system making the system capable of maintaining the evaporation rate even if a percentage of heat is lost via conduction to outside sources or materials. The slider will also prevent overheating of the system as it can block excess energy.

The cleansing ability of this system is very high due to the fact that it uses evaporation. Evaporated water kills bacteria and pathogens [12] and leaves residue such as salt and microplastics behind. However, according to Source 8, the hydrogels don't suffer from a build up in salt and the constant water flow results in the salt concentrating reaching equilibrium. This system will produce pure, clean and safe water. Additionally, the floatation capabilities of the system offer versatility giving it the possibility to not just work in small bodies of water but also function in lakes and even the ocean. A reliable water source out at sea could enable ships to carry more cargo instead of water reserves opening it to both military and commercial applications.

Future research includes the use of a DSC to determine the hydrogels evaporation enthalpy and also the synthesis of ten hydrogels to fill the multistage to enable the testing of the multistage's real world production rate. Further research can also be performed regarding the effect of differing temperatures and number of freeze-drying cycles on the hydrogels pore dispersion and size.

Conclusion*

This study designed and tested a system capable of producing 4.02 L hr^{-1} of clean water by utilizing a highly energy efficient multistage, energy decreasing hydrogels and a solar tracking concentrator. The system's 402 L hr^{-1} m^{-2} rate capability also enables the system to have a much greater production rate with more multistages or a multistage with a greater surface area which can be powered by a larger energy source. The system's ability to float and track the sun enables it to function anywhere on earth. Whether it be in poverty stricken developing countries, out at sea keeping sailors hydrated or even in your back-yard so that you can drink water knowing it is cleansed of salt, microplastics and bacteria. This study enables industry level efficiency partnered with robust engineering so it can be brought to the individual where it can make the difference between life and death.

References

[1] "Water and Sanitation – United Nations Sustainable Development." *United Nations*, United Nations, www.un.org/sustainabledevelopment/water-and-sanitation/.

[2] California-Great Basin, Bureau of Reclamation. "Central California Area Office." *Water Facts - Worldwide Water Supply | ARWEC| CCAO | Area Offices | California-Great Basin | Bureau of Reclamation*, 4 Nov. 2020,www.usbr.gov/mp/arwec/water-facts-ww-water-sup.html#:~:text=3%25%20of%20the%20earth's%20water,extracted%20at%20an%20affordable%20cost.

[3] Gabriel Filippelli, Indiana University – Purdue University Indianapolis. "Climate Change Threatens Drinking Water Quality Across the Great Lakes." *Discover Magazine*, Discover Magazine, 29 Apr. 2020, www.discovermagazine.com/environment/climate-change-threatens-drinking-water-quality-across-the-great-lakes.

[4] Robbins, Jim. "Desalination Is Booming as Cities Run out of Water." *Wired*, Conde Nast, 26 June 2019, 9:00 AM, www.wired.com/story/desalination-is-booming-as-cities-run-out-of-water/.

[5] "Climate Change." *Amazon Aid Foundation*, 25 Feb. 2018, amazonaid.org/threats-to-the-amazon/climate-change/#:~:text=The%20Amazon%20forest%20is%20a,much%20of%20the%20world's%20biodiversity.

[6] May, Sue Chen 26, et al. "How to Filter and Remove Microplastics from Tap Water? - TAPP Water." *USA*, 10 Feb. 2021,

[7] Reports, Consumer. "You're Literally Eating Microplastics. How You Can Cut down Exposure to Them." *The Washington Post*, WP Company, 7 Oct. 2019, www.washingtonpost.com/health/youre-literally-eating-microplastics-how-you-can-cut-down-exposure-to-them/2019/10/04/22ebdfb6-e17a-11e9-8dc8-498eabc129a0_story.html.

[8] Zhao, X., et al. (2019) Architecting highly hydratable polymer networks to tune the water state for solar water purification. American Association for the Advancement of Science, vol. 5, no. 6, doi:10.1126/sciadv.aaw5484.

[9] Lara, R., et al. (2017) Influence of freezing temperature and deacetylation degree on the performance of freeze-dried chitosan scaffolds towards cartilage tissue engineering. Science Direct, vol. 95, pp. 232-240, ISSN 0014-3057.

[10] Xu, Z., et al. (2020) Ultrahigh-Efficiency Desalination via a Thermally-Localized Multistage Solar Still. Energy & Environmental Science, vol. 13, no. 3, pp. 830– 839., doi:10.1039/c9ee04122b.

[11] Boundless. "Boundless Physics." *Lumen*, courses.lumenlearning.com/boundless-physics/chapter/specific-heat/#:~:text=The%20heat%20capacity%20and%20the,phase%20of%20a%20given%20substance.

[12]"Department of Health." *Boil Water Response-Information for the Public Health Professional*, Nov. 2018, www.health.ny.gov/environmental/water/drinking/boilwater/response_information_public_health_professional.htm.